Experimental Realization of Optimal Energy Storage in Resonators Embedded in Scattering Media

Philipp Hougne, Rémi Sobry, Olivier Legrand, Fabrice Mortessagne, Ulrich Kuhl, Matthieu Davy

Experimental realization of optimal energy storage in resonators embedded in scattering media

Philipp del Hougne Rémi Sobry Olivier Legrand Fabrice Mortessagne Ulrich Kuhl Matthieu Davy

Dr. P. del Hougne, Prof. O. Legrand, Prof. F. Mortessagne, Prof. U. Kuhl
Institut de Physique de Nice, CNRS UMR 7010, Université Côte d'Azur, 06108 Nice, France
Dr. P. del Hougne, R. Sobry, Dr. M. Davy
Univ Rennes, CNRS, Institut d'Électronique et des Technologies du numéRique, UMR–6164, F-35000 Rennes, France

Keywords: *Complex Scattering Media, Wavefront Shaping, Energy Storage, Resonator, Non-invasive Focusing*

The ability to enhance light-matter interactions by increasing the energy stored in optical resonators is inherently dependent on the resonators' coupling to the incident wavefront. In practice, weak coupling may result from resonators' irregular shapes and/or the scrambling of waves in the surrounding scattering environment. Here, a blind and non-invasive wavefront shaping technique providing optimal coupling to resonators is presented. The coherent control of the incident wavefront relies on the lengthening of delay times of waves efficiently exciting the resonator. Using a modal approach, the optimality of the proposed technique is proven and its limitations are quantified. The proposed concept is demonstrated in microwave experiments by injecting in-situ optimal wavefronts that maximize the energy stored in high-permittivity dielectric scatterers and extended leaky cavities embedded in a complex environment. The introduced framework is expected to find important applications in the enhancement of light-matter interactions in photonic materials as well as to enhance energy harvesting.

1 Introduction

Light incident upon a photonic resonator can be efficiently trapped by a long-lived mode if the light's frequency is within a narrow interval around the resonance. Since the energy stored in the resonator is proportional to the light's dwell time [1, 2, 3, 4], light confinement in photonic resonators constitutes an important mechanism to enhance light-matter interactions, for instance, to generate non-linear optical effects. Photonic resonators can take the form of optical microcavities [5, 6, 7, 8], nanocavities [9, 10] or Anderson-localized modes in disordered crystals [11, 12, 13], to name a few examples, and are also crucial to boost the absorption rate in light harvesting schemes [14, 15, 16, 17]. However, coupling light incident from the far-field to an optical resonator is a major challenge in many practical scenarios where (i) the resonator's shape is unknown or irregular and/or (ii) the resonator is embedded in a complex scattering environment. The latter completely scrambles the incident wavefront such that its coupling to the resonator, and consequently the energy storage, is dramatically reduced.

To counteract the effects of this scrambling, many wavefront shaping (WFS) techniques have been developed within the last decade that rely on tailoring the wavefront incident on a complex medium to coherently control wave propagation within the medium [18, 3]. In its simplest form, WFS may enhance energy storage in a point-like resonator embedded in a complex medium by focusing the wave field on its location. To determine how the incident wavefront should be shaped, such schemes must access in some way information about the wave field at the resonator's location. To circumvent the need for direct field measurements, a number of proposals indirectly obtain this information by implanting a guide-star at the target location [19, 20], by creating a virtual guide-star with multi-wave approaches [21, 22], by relying on a non-linear response at the target position [23, 24] or on a parametric variation of the target [25, 26, 27, 28].

None of these approaches enables blind and non-invasive focusing on the target. If, however, the target is known to be resonant, an alternative approach to couple energy into an embedded resonator without relying on any of the above-described conditions, and moreover also applicable to extended resonators, is related to the impact of the resonator's presence on the dwell time of waves that interacted with it. The Wigner-Smith time-delay operator (WSO) provides a blind and non-invasive tool to determine an incoming wavefront that optimizes the delay time [29, 30, 31, 32, 33, 34]. As long as the resonator's quality factor is clearly superior to that of the surrounding medium, the eigenstate of the WSO associated with the largest delay time may strongly increase the energy stored in the resonator [4]. Note that our blind and non-invasive approach sharply differs from Refs. [27, 28] which leverage a *generalized* version of the Wigner-Smith operator in which the frequency is replaced by a local parameter of the target (position, orientation, refractive index, ...) that has to be altered in-situ to determine the wavefront to be injected. Here, we begin by theoretically proving the optimality of injecting the first time-delay eigenstate to couple waves to a resonator embedded within a scattering medium. Then, we experimentally demonstrate the technique in the microwave domain: By injecting the optimal wavefronts in-situ, we observe a corresponding enhancement of the stored energy for a dielectric cylinder as well as for an extended leaky cavity, each embedded in a complex scattering environment. Finally, we quantify the technique's limitations when the quality factors of resonator and medium become comparable.

2 Theory

2.1 Wigner-Smith time-delay operator

The delay time of waves travelling through the medium carries key information about non-cooperative resonant inclusions. By identifying the wavefront that maximizes the delay time between incoming and outgoing waves, the time-delay signature of an embedded resonators can be leveraged to optimally excite the resonator and store energy within its volume. The delay time of outgoing waves $E_o = S(\omega)E_i$ for an incoming wavefront E_i is formally given by [4]

$$\tau(\omega, E_i) = -i\frac{E_o^\dagger \frac{\partial E_o}{\partial \omega}}{||E_o||^2} = -i\frac{E_i^\dagger S^\dagger(\omega)\frac{\partial S(\omega)}{\partial \omega}E_i}{E_i^\dagger S^\dagger(\omega)S(\omega)E_i}. \tag{1}$$

The scattering matrix $S(\omega)$ gives the fullest account of transmitted and reflected field coefficients between the channels coupled to the system. For systems with flux-conservation, the scattering matrix is unitary, $S^\dagger S = 1$, so that for a normalized incoming wavefront the definition in Eq. 1 coincides with the delay time $\tau(\omega, E_i) = E_i^\dagger Q(\omega) E_i$ found using the WSO [35, 1, 36, 37]

$$Q(\omega) = -iS^{-1}(\omega)\frac{\partial S(\omega)}{\partial \omega}. \tag{2}$$

The WSO generalizes the phase derivative of the transmission amplitude giving the delay time of waves in 1D systems [38] to multi-channel systems. The eigenvalues of $Q(\omega)$ verifying $q_i^\dagger Q(\omega) = \tau_i q_i^\dagger$ are known as the proper delay times. They are real and give well-defined delay times obtained upon using the eigenvectors of $Q(\omega)$ as incident wavefronts: $\tau_i = \tau(\omega, q_i)$. An eigenstate of the operator $Q(\omega)$ is referred to as time-delay eigenstate (TDE) since injecting this state into the system will result in a specific time delay $Re[\tau]$, where tau is the eigenvalue associated with the eigenstate. The eigenvector associated with the largest proper delay time hence provides the incoming wavefront optimizing the delay time and the optimal energy stored within the medium [4].
The generality of the scattering-matrix formalism implies that our technique does not depend on the spatial arrangement of the channels; it can be used equally well with an array of channels or an ensemble of randomly placed channels, both in 2D and 3D systems. However, in many experimental setups, energy can only be injected through a subset of channels on one side of the medium. The WSO is then constructed from a measurement of the transmission matrix (TM) $t(\omega)$ or reflection matrix (RM) $r(\omega)$. $t(\omega)$ and $r(\omega)$ are non-unitary matrices so that the corresponding WSOs, $Q_t(\omega) = -it^{-1}(\omega)\frac{\partial t(\omega)}{\partial \omega}$ and $Q_r(\omega) = -ir^{-1}(\omega)\frac{\partial r(\omega)}{\partial \omega}$, respectively, are non-Hermitian with complex eigenvalues $\tilde{\tau}_i$. Neverthless, the real part of $\tilde{\tau}_i$ gives the frequency derivative of a scattering phase related to a delay time [39, 34]. The imaginary part of $\tilde{\tau}_i$ reflects the variation of transmitted or reflected intensities with frequency.

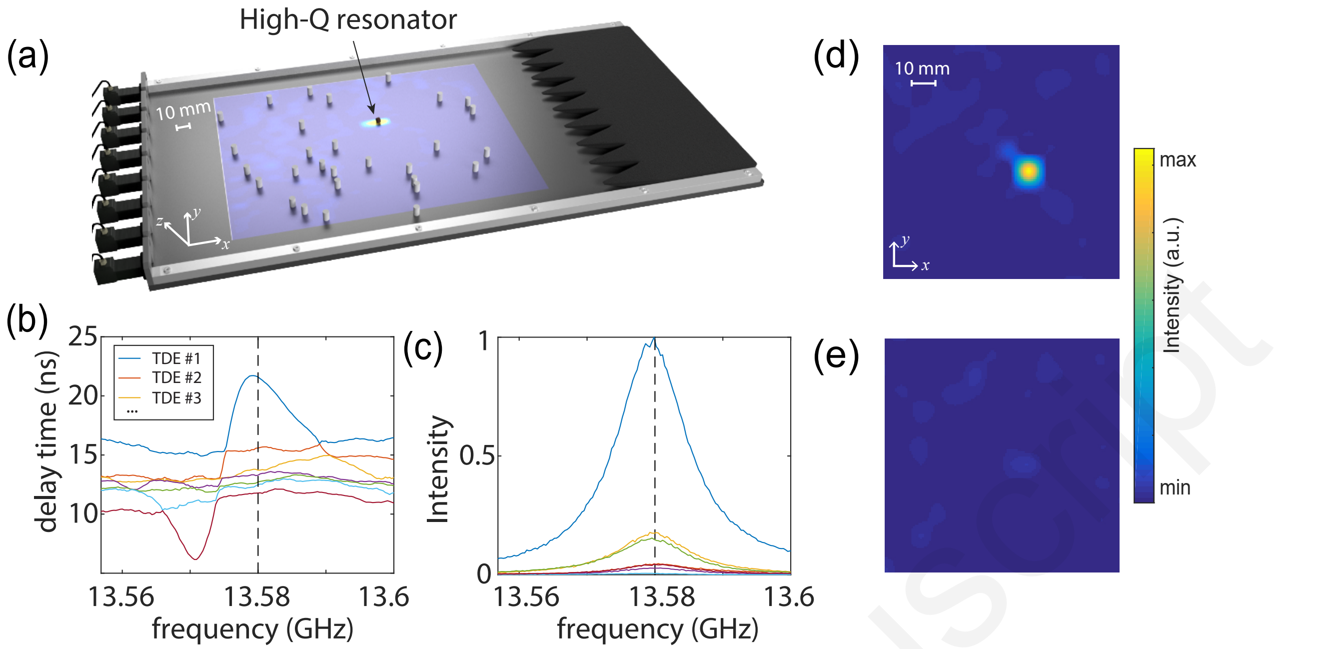

Figure 1: (a) Schematic of experimental setup. The waveguide's top plate is removed to show the interior. The projected intensity map shows the blind focusing on an embedded resonator achieved by injecting the first TDE of the RM. (b,c) Spectra of the real part of the time-delay eigenvalues $\tilde{\tau}_n(\omega)$ (b) and intensity at the dielectric resonator's location measured upon injecting in-situ the TDEs at $f_0 = 13.58$ GHz (the first TDE's eigenvalue peaks at f_0, see black dashed line) (c). (d,e) Spatial distribution of energy density of the first (d) and second (e) TDE. These maps are obtained via a two-dimensional interpolation of the field measurements on a grid of holes with spacing of 8 mm in the vicinity of the resonator (see Supporting Information for technical details).

2.2 Optimality

For the example of $Q_r(\omega)$ we now demonstrate using a modal perspective that the TDE with the largest eigenvalue is the optimal wavefront for maximal coupling to an embedded resonator. The quasi-normal modes (referred to as mode in the following) are the eigenfunctions $\phi_m(r)$ that are solutions of the wave equation with outgoing boundary conditions. The modes are associated with spectral resonances characterized by complex eigenfrequencies $\tilde{\omega}_m = \omega_m - i\Gamma_m/2$ with central frequency ω_m. The linewidth Γ_m is inversely proportional to the modal decay rate $2/\Gamma_m$ or equivalently to its quality factor $\mathcal{Q}_m = 2\omega_m/\Gamma_m$. We analyze the TDEs of $Q_r(\omega)$ near the resonance with the resonator's nth mode. We decompose $r(\omega)$ into a superposition of a background contribution, $r_0(\omega)$, and a resonant modal term with Lorentzian lineshape expressed as $r_n(\omega) = -iW_n[\omega - \tilde{\omega}_n]^{-1}W_n^T$, so that $r(\omega) = r_0(\omega) + r_n(\omega)$. The vector W_n is the projection of the corresponding eigenfunction $\phi_n(r)$ onto the channels. Since $r_n(\omega)$ is a matrix of rank one, the Sherman–Morrison formula [40] yields $r^{-1}(\omega) = r_0^{-1}(\omega) - [r_0^{-1}(\omega)r_n(\omega)r_0^{-1}(\omega)]/[1+\kappa(\omega)]$, where $\kappa(\omega) = \mathrm{Tr}(r_0^{-1}(\omega)r_n(\omega))$. Using that $\partial r_n(\omega)/\partial\omega = -r_n(\omega)/(\omega - \tilde{\omega}_n)$, straightforward algebraic manipulations yield the expression of the WSO at the resonance $\omega = \omega_n$ [1]

$$Q_r(\omega_n) = Q_{r_0}(\omega_n) + \frac{r_0^{-1}(\omega_n)r_n(\omega_n)}{1+\kappa(\omega_n)}\left[\frac{2}{\Gamma_n} - Q_{r_0}(\omega_n)\right]. \quad (3)$$

$Q_{r_0}(\omega_n)$ is the WSO applied to the background contribution. The contribution associated with the resonator $Q_n(\omega_n) = 2r_0^{-1}(\omega_n)r_n(\omega_n)/[\Gamma_n(1+\kappa(\omega_n))]$ is also a rank one matrix. The left eigenvector of $Q_n(\omega)$ which verifies $q_1^\dagger Q_n(\omega_n) = \tilde{\tau}_1 q_1^\dagger$ is given by $q_1 = W_n^*/||W_n||$. q_1 therefore provides maximal excitation of this mode [41]. The associated eigenvalue is $\tilde{\tau}_1 = (2/\Gamma_n)[\kappa(\omega_n)/(1+\kappa(\omega_n))]$.
We now assume that the modes can be separated into two categories: (i) short-lived modes (small quality factors) of the surrounding environment with eigenfunctions which extend throughout the system and

[1] See Supporting Information for technical details details on the radiofrequency chain, on the proof of Eq. (3), for a demonstration of selective focusing on two resonators, and for additional numerical simulations.

weakly interact with the resonator; and (ii) long-lived modes spatially localized on the resonator whose quality factors significantly exceed those of the first category. The parameter $\kappa(\omega_n) = -2W_n^T r_0^{-1} W_n/\Gamma_n$ depends on the system of interest but can be evaluated in absence of absorption and for a complete control on the channels coupled to the system, in which case $r^{-1} = r^{\dagger}$. The Sherman–Morrison formula gives $\kappa(\omega_n)/(1+\kappa(\omega_n)) = Tr(r^{\dagger} r_n)$. Using the orthogonality between the resonator's mode ϕ_n and the background's modes $\phi_{m\neq n}$ (see Supporting Information), we obtain $\kappa(\omega_n) = -2$ and $\tilde{\tau}_1 = (4/\Gamma_n)$, which is the contribution of a mode at resonance to $Tr(Q)$ [42, 43]. When the resonator's contribution $4/\Gamma_n$ is larger than the first eigenvalue of $Q_{r_0}(\omega_n)$, the first eigenstate of $Q_r(\omega_n)$ coincides with the eigenstate of $Q_n(\omega_n)$ and injecting the left eigenvector q_1 of $Q_r(\omega_n)$ provides maximal excitation of the resonator. In the last section, we quantitatively discuss limitations of our approach that arise for systems for which the linewidths associated with background modes are smaller than Γ_n.

3 Experimental Demonstration

3.1 Coupling to a single resonator

Having established the theory, our first experiment demonstrates optimal focusing on a single high-$\mathcal{Q}$ dielectric cylinder with a permittivity $\epsilon \sim 37$ [44], embedded in a complex environment. As shown in Figure 1, the latter is a quasi-two-dimensional multimode waveguide (in the considered frequency range) that is filled with 30 randomly placed low-$\mathcal{Q}$ scatterers (teflon cylinders, diameter 5 mm, $\epsilon \sim 2.07$). One waveguide end is covered with absorbing foam to mimic open boundary conditions while an array of $N = 8$ coax antennas is located at the other end. The radiofrequency chain including IQ-modulators behind each antenna is designed to allow simultaneously the in-situ injection of waves with tailored amplitude and phase profile and the reception of the return signals (see Supporting Information for details). These unique capabilities make this microwave setup an ideal candidate for a proof-of-concept demonstration.
First, we measure the reflection matrix $r(\omega)$ associated with the antenna array between 13 and 14 GHz and calculate the WSO $Q_r(\omega)$. A peak is observed in Figure 1(b) at $f_0 = 13.58$ GHz on the spectrum of the real part of the first eigenvalue $\tilde{\tau}_1$. The delay time $\tilde{\tau}_1(\omega_0)$ reaches 21.5 ns. This corresponds to a resonator's $\mathcal{Q}$-factor of $\mathcal{Q}_m \sim 917$. $\tilde{\tau}_1(\omega_0)$ clearly dominates the other contributions that do not exceed 16 ns at f_0. The measured average delay time over the frequency range is $\langle\tau\rangle = 13.7$ ns. Second, we inject in-situ the normalized left eigenvector q_1 of the WSO corresponding to the largest delay time at f_0. To measure the spatial distribution of the intensity, we scan the excited field in the scattering medium with a minimally invasive antenna inserted via small holes in the waveguide's top plate. The result shown in Figure 1(d) evidences strong focusing at the resonator's location. Relative to the average intensity at that location for the other eigenvectors, the intensity is enhanced by a factor of $\eta = 10.2$. This enhancement is close to its expected value in random media related to the number incoming channels N by, $\eta = N = 8$. We also inject the other TDEs into the system. The obtained intensity distribution for the second TDE is shown in Figure 1(e), the other field maps are provided in the Supporting Information. The intensity at the resonator's location is slightly stronger than for the surrounding background as a consequence of the resonator's high $\mathcal{Q}$-factor, but the incoming wavefront does not result in a proper focal spot. This is confirmed by spectra of the intensity at the resonator's location for the first seven TDEs in Figure 1(c).
In Figure 2 we benchmark the achieved focusing intensity with our blind non-invasive scheme against the optimal value attainable with an invasive phase-conjugation scheme. Our proposed scheme achieves 90 % of the maximum achievable intensity obtained by phase-conjugating the field coefficients between the channels and the scanning antenna inserted via the hole above the resonator [45]. We attribute the slight difference to the non-homogeneous energy density distribution within the resonator.
We now compare the focused intensity to the first and last reflection eigenchannels in Figure 2. In the single scattering regime, the first eigenchannel of the matrix $r^{\dagger}(\omega)r(\omega)$, known as the time-reversal operator, would also provide focusing on the strongest scatterer, here, the resonator [46]. However, the cor-

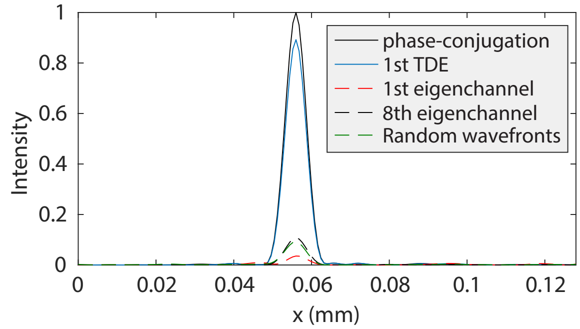

Figure 2: Comparison of the focused intensity using a phase-conjugation technique (black line), the first TDE (blue line), the first (red dashed line) and last (black dashed line) reflection eigenchannels and its average over 100 random incoming wavefronts.

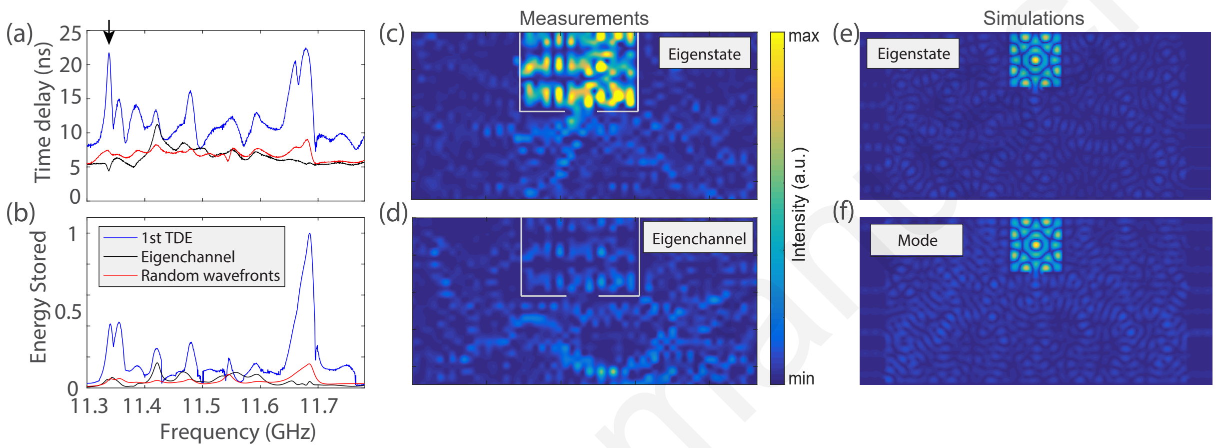

Figure 3: Energy storage in an embedded extended leaky cavity resonator (L_c = 104 mm, W_c = 152 mm). (a,b) Spectra of the delay time (a) and energy stored within the cavity (b) for the first TDE, the first transmission eigenchannel and an average over 200 random incoming wavefront. (c,d) Energy density distributions within the medium at 11.34 GHz for the first TDE (c) and the first transmission eigenchannel (d), respectively. (e,f) Spatial distribution for the first TDE (e) and the mode at resonance (f) obtained in simulation for the same geometry.

respondence fails in the multiple scattering regime as mainly the first scatterers located between the antennas and the resonator are excited [47]. We also observe that the intensity on the resonator remains small if the last eigenchannel corresponding to minimal reflections is excited. For systems with perfectly controlled openings, minimizing the outgoing intensity coherently enhances absorption within the medium [48, 49, 50, 51] so that the scatterers with largest $\mathcal{Q}$-factors and hence largest absorption rates may be preferentially excited [52]. However, we control only a small fraction of incoming and outgoing channels since the system is fully opened at the right side. The eigenchannel with minimal reflection is therefore mainly associated with an increase of transmission from left to right.

3.2 Coupling to an extended resonator

We now consider extended resonators with dimensions greater than the diffraction limit. Identifying the wavefront that optimally couples to extended resonators, here a rectangular leaky cavity with aluminum walls and an opening of 25 mm $\sim 1.05\lambda$ at 11.5 GHz, is non-trivial even without a surrounding scattering medium. At the same time, to demonstrate the versatility of our approach, we now work with $t(\omega)$ rather than $r(\omega)$. To that end, we replace the absorbing foam on one end of the waveguide with another array of $N = 8$ antennas. We place small pieces of absorbing material in front of the metallic walls between all neighboring antennas to prevent the waveguide from having strong internal reflections (see also discussion below).

We compute the TDEs by applying the WSO to the TM, $Q_t = -it^{-1}(\omega)\frac{\partial t(\omega)}{\partial \omega}$. We obtain the correspond-

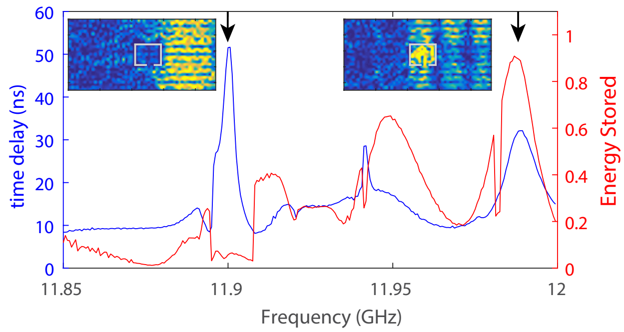

Figure 4: Delay time and energy stored within an extended cavity ($L_c = 56$ mm, $W_c = 72$ mm, 15 mm aperture) for the first TDE. The insets show intensity distributions of the TDE at $f_0 = 11.905$ GHz and $f_0 = 11.98$ GHz.

ing energy density distributions displayed in Figure 3, this time by analytically injecting the eigenvectors of the WSO into a second transmission matrix linking the input ports to grid positions within the sample. We calculate the energy stored within the resonator for each TDE, $U_n(\omega)$, by integrating the field intensity over the surface of the resonator. The variation of $U_1(\omega)$ with frequency is seen in Figure 3(b) to be highly correlated (similarity coefficient 0.68) with the variation of the real part of $\tilde{\tau}_1(\omega)$. The delay time and the energy stored within the cavity for the first TDE are enhanced relative to their averages for random illuminations, with maximal factors of 6.25 and 5.71 at 11.68 GHz.

The enhancement of the stored energy relative to random wavefronts shown in Figure 3(b) is confirmed by the energy density distribution in Figure 3(c). In contrast to the first eigenchannel of $t^\dagger(\omega)t(\omega)$ for which the wave follows scattering paths around the cavity (see Figure 3(d)), the wave in the first TDE is seen to strongly penetrate into the cavity with a spatial distribution reminiscent of a regular cavity's eigenfunction. As shown in our theoretical analysis, the incoming wavefront indeed maximally excites the resonant mode at its resonance. We confirm the correspondence between the first TDE and the mode at resonance in numerical simulations reproducing the experimental setup: the spatial distributions in Figure 3(e,f) are in excellent agreement within the resonator. In our simulations, the energy stored in the resonator with the first TDE reaches 99.5% of its optimal value.

3.3 Limitations

Finally, we consider the limitations of our blind-focusing technique. We assumed up to now that the eigenvalue associated with the resonator $(4/\Gamma_n)$ is larger than the maximal delay time associated with the surrounding medium so that the peaks in the first eigenvalue of the WSO can be identified as a signature of the resonator. However, for resonators associated with delay times smaller than the maximal delay time of the environment, Eq. (3) demonstrates that the first TDE corresponds to the first eigenstate of the background contribution $Q_{r_0}(\omega)$ which will not excite the resonator. To quantify this limitation, we assume that the proper delay times τ of the surrounding environment can be described by a distribution $P(\tau)$. Maximal excitation of the resonator hence requires that $4/\Gamma_n > max(\tau)$. For a chaotic cavity without resonant inclusion, $P(\tau)$ has a finite support with an upper bound τ_+ which scales linearly with the average delay time $\langle\tau\rangle$ as $\tau_+ = (3+\sqrt{8})\langle\tau\rangle$ [36, 53, 54]. In a chaotic cavity with M fully coupled channels, $\langle\tau\rangle = \tau_H/M$, where the Heisenberg time τ_H is the inverse of the average level spacing: $\tau_H = 1/\Delta$. Our focusing technique is hence efficient as long as $4/\Gamma_n \gg \langle\tau\rangle$. This was the case in Figure 3 for which we estimate $\langle\tau\rangle \sim 3.5$ ns. In a diffusive slab with mean free path ℓ and thickness $L \gg \ell$, $P(\tau)$ also exhibits an upper bound τ_+ which scales as $\tau_+ \sim L^2/(c_0\ell)$ [55, 4] so that the limits of our technique are quantitatively known, too.

To illustrate limitations in high-$\mathcal{Q}$ environments, we reduce the size of the cavity placed in the middle of the waveguide (see Figure 4). We also remove the pieces of absorbing foam between neighboring antennas at the two waveguide ends so that internal reflections appear between the openings due to metallic boundary conditions. The regular shape of the waveguide closed at both ends results in very long-lived modes not associated with the resonant target. In an integrable cavity, the distribution of proper delay times decays algebraically for $\tau \gg \langle\tau\rangle$ and does not exhibit a cutoff as in chaotic cavities [56]. $\langle\tau\rangle$ increases to 6.7 ns and we observe in Figure 4 that a direct mapping between peaks in $\tilde{\tau}_1$ and an enhancement of the energy stored within the resonator is no longer possible. The peak given by $\tilde{\tau}_1 \sim 32$ ns at $f_0 = 11.98$ GHz still corresponds to a peak of $U_1(\omega)$. However, the first TDE at $f_0 = 11.905$ GHz with $\tilde{\tau}_1 \sim 53$ ns corresponds to a long-lived mode trapped between the waveguide's top and bottom boundaries which very weakly penetrates into the cavity resonator. The delay time of this mode largely exceeds the delay time associated with the resonator at this frequency. Overall, the correlation between the spectra of $\tilde{\tau}_1$ and $U_1(\omega)$ is now only 0.33.

4 Conclusion

To summarize, we experimentally demonstrated optimal blind and non-invasive focusing on a resonant inclusion in a complex scattering environment by controlling delay times of transmitted and reflected waves in a multi-channel system. For the case of multiple resonant targets, we describe an example of selective focusing on two resonators in the Supporting Information; a thorough investigation of multi-target focusing with our technique is left for future work. Another question for future research is related to the possibility of further enhancements by shaping the incident wavefront not only in space but additionally in time. Given that the resonant target's linewidth must be much thinner than a typical resonance in the surrounding scattering medium, it appears impossible to find two or more frequencies capable of exciting the target's resonance that would propagate "independently" through the scattering medium. Nonetheless, this limitation may be circumvented by leveraging higher harmonics of the targeted resonator. Our approach demonstrated in the microwave range can be extended to optics, acoustics and seismology. We expect these results to trigger new schemes to enhance energy harvesting and non-linear effects in photonic and phononic materials [57]. Our framework may also open new perspectives for coherent perfect absorption in random media [51, 58, 52, 59, 60], to control random lasing [61] and for deep-imaging through highly scattering samples [62].

Supporting Information
Supporting Information is available from the Wiley Online Library or from the author.

Acknowledgements
This publication was supported by the European Union through the European Regional Development Fund (ERDF), by the French region of Brittany and Rennes Métropole through the CPER Project SOPHIE/STIC & Ondes and by the French "Agence Nationale de la Recherche" under reference ANR-17-ASTR-0017. The authors acknowledge C. Leconte for her help in automating the field scan and P.E. Davy for the 3D rendering of the experimental setup. M.D. acknowledges the "Institut Universitaire de France".

Author Contributions
The project was initiated and conceptualized by M.D. The experiments were carried out by P.d.H and M.D. and the simulations were performed by R.S. and M.D. All authors thoroughly discussed the results. The manuscript was written by P.d.H. and M.D. and reviewed by all authors.

References

[1] F. T. Smith, *Phys. Rev.* **1960**, *118*, 1 349.

[2] A. Lagendijk, B. A. Van Tiggelen, *Phys. Rep.* **1996**, *270*, 3 143.

[3] S. Rotter, S. Gigan, *Rev. Mod. Phys.* **2017**, *89*, 1 015005.

[4] M. Durand, S. M. Popoff, R. Carminati, A. Goetschy, *Phys. Rev. Lett.* **2019**, *123*, 24 243901.

[5] R. K. Chang, A. J. Campillo, *Optical Processes in Microcavities*, volume 3, World Scientific, **1996**.

[6] K. J. Vahala, *Nature* **2003**, *424*, 6950 839.

[7] C. Liu, A. Di Falco, D. Molinari, Y. Khan, B. S. Ooi, T. F. Krauss, A. Fratalocchi, *Nat. Photonics* **2013**, *7* 473.

[8] H. Cao, J. Wiersig, *Rev. Mod. Phys.* **2015**, *87*, 1 61.

[9] Y. Akahane, T. Asano, B.-S. Song, S. Noda, *Nature* **2003**, *425*, 6961 944.

[10] B.-S. Song, S. Noda, T. Asano, Y. Akahane, *Nat. Mater.* **2005**, *4*, 3 207.

[11] A. Chabanov, M. Stoytchev, A. Genack, *Nature* **2000**, *404*, 6780 850.

[12] P. Sebbah, B. Hu, J. M. Klosner, A. Z. Genack, *Phys. Rev. Lett.* **2006**, *96*, 18 183902.

[13] L. Sapienza, H. Thyrrestrup, S. Stobbe, P. D. Garcia, S. Smolka, P. Lodahl, *Science* **2010**, *327*, 5971 1352.

[14] E. Yablonovitch, G. D. Cody, *IEEE Trans. Electron. Devices* **1982**, *29*, 2 300.

[15] K. Vynck, M. Burresi, F. Riboli, D. S. Wiersma, *Nat. Mater.* **2012**, *11*, 12 1017.

[16] Y. Yao, J. Yao, V. K. Narasimhan, Z. Ruan, C. Xie, S. Fan, Y. Cui, *Nat. Commun.* **2012**, *3*, 1 664.

[17] M. Garín, R. Fenollosa, R. Alcubilla, L. Shi, L. Marsal, F. Meseguer, *Nat. Commun.* **2014**, *5* 3440.

[18] A. P. Mosk, A. Lagendijk, G. Lerosey, M. Fink, *Nat. Photonics* **2012**, *6*, 5 283.

[19] I. M. Vellekoop, E. Van Putten, A. Lagendijk, A. Mosk, *Opt. Express* **2008**, *16*, 1 67.

[20] R. Horstmeyer, H. Ruan, C. Yang, *Nat. Photonics* **2015**, *9*, 9 563.

[21] B. Larrat, M. Pernot, G. Montaldo, M. Fink, M. Tanter, *IEEE Trans. Ultrason. Ferroelectr. Freq. Control.* **2010**, *57*, 8 1734.

[22] T. Chaigne, O. Katz, A. C. Boccara, M. Fink, E. Bossy, S. Gigan, *Nat. Photonics* **2014**, *8*, 1 58.

[23] O. Katz, E. Small, Y. Guan, Y. Silberberg, *Optica* **2014**, *1*, 3 170.

[24] P. del Hougne, M. Fink, G. Lerosey, *Phys. Rev. Applied* **2017**, *8*, 6 061001.

[25] C. Ma, X. Xu, Y. Liu, L. V. Wang, *Nat. Photonics* **2014**, *8*, 12 931.

[26] E. H. Zhou, H. Ruan, C. Yang, B. Judkewitz, *Optica* **2014**, *1*, 4 227.

[27] P. Ambichl, A. Brandstötter, J. Böhm, M. Kühmayer, U. Kuhl, S. Rotter, *Phys. Rev. Lett.* **2017**, *119*, 3 033903.

[28] M. Horodynski, M. Kühmayer, A. Brandstötter, K. Pichler, Y. V. Fyodorov, U. Kuhl, S. Rotter, *Nat. Photonics* **2019**, 1–5.

[29] S. Rotter, P. Ambichl, F. Libisch, *Phys. Rev. Lett.* **2011**, *106*, 12 120602.

[30] J. Carpenter, B. J. Eggleton, J. Schröder, *Nat. Photonics* **2015**, *9*, 11 751.

[31] B. Gérardin, J. Laurent, P. Ambichl, C. Prada, S. Rotter, A. Aubry, *Phys. Rev. B* **2016**, *94*, 1 014209.

[32] W. Xiong, P. Ambichl, Y. Bromberg, B. Redding, S. Rotter, H. Cao, *Phys. Rev. Lett.* **2016**, *117*, 5 053901.

[33] P. Ambichl, W. Xiong, Y. Bromberg, B. Redding, H. Cao, S. Rotter, *Phys. Rev. X* **2017**, *7*, 4 041053, pRX.

[34] J. Böhm, A. Brandstötter, P. Ambichl, S. Rotter, U. Kuhl, *Phys. Rev. A* **2018**, *97*, 2 021801.

[35] E. P. Wigner, *Phys. Rev.* **1955**, *98*, 1 145.

[36] P. W. Brouwer, K. M. Frahm, C. W. J. Beenakker, *Phys. Rev. Lett.* **1997**, *78*, 25 4737.

[37] U. R. Patel, E. Michielssen, *arXiv:2003.06985* **2020**.

[38] Y. Avishai, Y. B. Band, *Phys. Rev. B* **1985**, *32*, 4 2674.

[39] S. Fan, J. M. Kahn, *Opt. Lett.* **2005**, *30*, 2 135.

[40] J. Sherman, W. J. Morrison, *Ann. Math. Stat.* **1950**, *21*, 1 124.

[41] M. Davy, A. Z. Genack, *Nat. Commun.* **2018**, *9*, 1 4714.

[42] N. Lehmann, D. Savin, V. Sokolov, H.-J. Sommers, *Physica D* **1995**, *86*, 4 572.

[43] A. Grabsch, D. V. Savin, C. Texier, *J. Phys. A* **2018**, *51*, 40 404001.

[44] D. Laurent, O. Legrand, P. Sebbah, C. Vanneste, F. Mortessagne, *Phys. Rev. Lett.* **2007**, *99*, 25 253902.

[45] I. M. Vellekoop, A. P. Mosk, *Phys. Rev. Lett.* **2008**, *101*, 12 120601.

[46] C. Prada, M. Fink, *Wave Motion* **1994**, *20*, 2 151.

[47] A. Aubry, A. Derode, *Phys. Rev. Lett.* **2009**, *102*, 8 084301.

[48] Y. D. Chong, A. D. Stone, *Phys. Rev. Lett.* **2011**, *107*, 16 163901.

[49] W. Wan, Y. Chong, L. Ge, H. Noh, A. D. Stone, H. Cao, *Science* **2011**, *331*, 6019 889.

[50] D. G. Baranov, A. Krasnok, T. Shegai, A. Alù, Y. Chong, *Nat. Rev. Materials* **2017**, *2*, 12 17064.

[51] K. Pichler, M. Kühmayer, J. Böhm, A. Brandstötter, P. Ambichl, U. Kuhl, S. Rotter, *Nature* **2019**, *567*, 7748 351.

[52] H. Li, S. Suwunnarat, T. Kottos, *Phys. Rev. B* **2018**, *98*, 4 041107.

[53] H.-J. Sommers, D. V. Savin, V. V. Sokolov, *Phys. Rev. Lett.* **2001**, *87*, 9 094101.

[54] T. Kottos, *J. Phys. A* **2005**, *38*, 49 10761.

[55] M. Davy, Z. Shi, J. Wang, X. Cheng, A. Z. Genack, *Phys. Rev. Lett.* **2015**, *114*, 3 033901.

[56] M. G. A. Crawford, P. W. Brouwer, *Phys. Rev. E* **2002**, *65*, 2 026221.

[57] L. Zhu, J. Wang, *Sci. Rep.* **2014**, *4* 7441.

[58] L. Chen, T. Kottos, S. M. Anlage, *arXiv:2001.00956* **2020**.

[59] M. F. Imani, D. R. Smith, P. del Hougne, *Adv. Funct. Mater.* **2020**, *TBA* 2005310.

[60] P. del Hougne, K. B. Yeo, P. Besnier, M. Davy, *arXiv:2010.06438* **2020**.

[61] H. Cao, *Waves Random Complex Media* **2003**, *13*, 3 1.

[62] S. Gigan, *Nat. Photonics* **2017**, *11*, 1 14.

Table of Contents

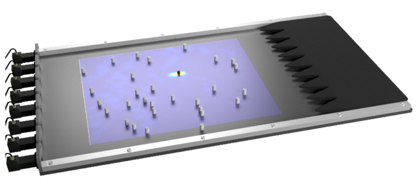

By leveraging the dwell-time enhancement of waves that interact with a resonator, waves can be focused on a resonator of arbitrary shape, even if it is embedded in a scattering medium at an unknown location. The optimality of this blind and non-invasive scheme is theoretically proven with a modal approach. The technique is demonstrated with experiments in the microwave domain.